Characterization of Titanium Dioxide Nanoparticles Using Molecular Dynamics Simulations

Pavan K. Naicker,*,†,‡ Peter T. Cummings,‡,§,⊥ Hengzhong Zhang,|| and Jillian F. Banfield||

Department of Chemistry, University of Cape Town, Private Bag Rondebosch, Cape Town, 7701, South Africa, Department of Chemical Engineering, Vanderbilt University, VU Station B 351604, Nashville, Tennessee 37235, Chemical Sciences Division, Oak Ridge National Laboratory, Oak Ridge, Tennessee 37831, Nanomaterials Theory Institute, Oak Ridge National Laboratory, Oak Ridge, Tennessee 37831, and Department of Earth and Planetary Science, University of California, Berkeley, California 94720

Received: February 24, 2005; In Final Form: June 6, 2005

Molecular dynamics simulations of titanium dioxide nanoparticles in the three commonly occurring phases (anatase, brookite, and rutile) are reported. The structural properties inferred by simulated X-ray diffraction patterns of the nanoparticles were investigated. The titanium−oxygen bond length as a function of size, phase, and temperature was determined and was found to be dependent on the coordination environment of the titanium and independent of phase and size. The equilibrium Ti−O bond length is 1.86 Å for a four-coordinated titanium ion, 1.92 Å for a five-coordinated titanium ion, and 1.94 Å for an octahedral titanium ion. Smaller nanoparticles are characterized by a higher fraction of titanium ions that are four and five coordinated, due to the larger surface area-to-volume ratios. The surface energies for anatase, rutile, and brookite particles were reported. The surface energy of the nanoparticle increases and approaches a constant value as the particle gets bigger. The surface energies of small rutile particles are higher than that for anatase particles of a similar size, consistent with anatase being the more stable phase of nanocrystalline titanium dioxide.

1. Introduction

Studies[1−3] on clusters of particles in the nanometer range have revealed some unusual bonding geometries. This, together with the considerable interest in nanoparticle processing, invites an examination of the effect of size on the structural properties of nanoparticles. Consequently the structural properties of nanoparticles is an area of active research.[4−17] An obvious feature of nanoparticles is the extreme surface area-to-volume ratio that affects the physical and chemical behavior of such systems. Furthermore, nanoparticles have been found to possess novel physical properties that can be commercially exploited; additionally metal oxide nanoparticles in particular are common byproducts of environmental oxidation processes.[13,18−21] There have been few studies on the finer structural details of metal oxide nanoparticles.[4,5,8,9,11,12,22] Other studies relate to controlling physicochemical and electronic properties of metal oxide nanoparticles.[14−17]

An ideal model compound for a study of metal oxide nanoparticles is titanium dioxide because of the abundance of literature on this compound.[6,9,10,12,18,22−31] Experimental[32,33] X-ray absorption fine structure (XAFS) data show that Ti−O bond lengths in nanocrystalline titanium dioxide are significantly different from the bulk phase value of 1.94 Å and can be as low as 1.79 Å. X-ray absorption near edge structure (XANES) data have been reported that indicate that the curvature of the surface causes a decrease in the coordination environment of the titanium ion[32−34] from the normal octahedral environment to an environment where it has a coordination number of 4 or 5. Accordingly, Ti−O bond lengths as well as coordination environments of the titanium ions were determined in this study with use of molecular simulation methods.

In this work nanoparticles in three commonly occurring phases of titanium dioxide (rutile, anatase, and brookite) ranging from 2 to 6 nm in size at 300 K were simulated via classical molecular dynamics. These particles were examined to determine the effect of size on phase stability. X-ray diffraction patterns were determined by using Debye functional analysis to see if any phase change occurs over the time scale of the simulations and to infer structural properties. Simulations of nanoparticles ranging from 2 to 4 nm in all three phases at temperatures ranging from 300 to 2500 K were also carried out to determine the effect of temperature on the properties of these nanoparticles.

The formation of a surface on these nanoparticles is important, as it is the main factor controlling the difference in behavior between bulk and nanocrystalline titanium dioxide. The surface energies of finite size particles are different from the surface energies of planar surfaces, as the curvature of the finite size particles in addition to their shape has to be accounted for. In this work the surface energies as a function of phase and size were calculated. The surface energies of the nanoparticles were compared to the surface energies of planar surfaces. To the authors knowledge this work represents the first surface energy calculations for titanium dioxide nanoparticles.

Previous simulations involving titanium dioxide nanoparticles include the work by Collins et al.,[31,35] who performed simulations on 1245 atom rutile clusters at temperatures ranging from 1000 to 3000 K. Their results show that the structural properties of the cluster are strongly influenced by the surface. Collins et al.[31,35] also report the clusters showing strong evidence of faceting with the [110], [100], and [101] surfaces being present.

* Address correspondence to this author. Phone: + 2721-650-4134. Fax: +2721-689-7499. E-mail: pnaicker@science.uct.ac.za.
† University of Cape Town.
‡ Vanderbilt University.
§ Chemical Sciences Division, Oak Ridge National Laboratory.
⊥ Nanomaterials Theory Institute, Oak Ridge National Laboratory.
|| University of California.

10.1021/jp050963q CCC: $30.25
Published on Web 07/26/2005

TABLE 1: Interaction Parameters for Eq 1[40]

interaction	A_{ij}, kcal mol^{-1}	ρ_{ij}, Å	C_{ij}, kcal mol^{-1} Å^{-6}
Ti−Ti	717654	0.154	120.997
Ti−O	391053	0.194	290.392
O−O	271719	0.234	696.941

In this work we go further and all three phases (rutile, anatase, and brookite) of titanium dioxide are studied and particles ranging in size from 2 to 6 nm are investigated. The studies in this work also include a wider temperature range.

This paper is organized as follows. In the next section the simulation method and the force field used in this work are presented. The method used to generate starting configurations and the method used to calculate simulated X-ray diffraction patterns are also reported in this section. In section 3 the structural and thermodynamic properties are discussed. This is followed in the last section by a summary of the main conclusions of this work.

2. Simulation Details

2.1. The Force Field Selection. A survey of the literature has indicated that several force fields for titanium dioxide and titanium oxide have been published.[23−26,29,30,36−43] A detailed analysis of the different available force fields has been published by Smith and co-workers.[39] They conclude that the force field of Matsui and Akaogi[40] is the most suitable of the available force fields for use in classical molecular dynamics simulation. This is in agreement with Swamy et al.,[28,29] who have compared a variable-charge force field for titanium dioxide to the force field of Matsui and Akaogi.[40] They found that in some instances the force field of Matsui and Akaogi[40] performs better than the more complicated variable charge force field. Consequently in this work we used the Matsui−Akaogi force field. The force field is a simple atomistic force field that we have rewritten in a site−site interaction form:

$$U(r_{ij}) = A_{ij}\exp\left(-\frac{r_{ij}}{\rho_{ij}}\right) - \frac{C_{ij}}{r_{ij}^{6}} + \frac{q_i q_j}{r_{ij}} \qquad (1)$$

where $U(r_{ij})$ is the interaction energy between sites i and j and the parameters A_{ij}, ρ_{ij}, and C_{ij} are listed in Table 1. The charges q_i for titanium and oxygen are +2.196 and −1.098, respectively, in atomic units.

2.2. Simulation Method. Molecular dynamics simulations have been carried out with the classical molecular dynamics code DL_POLY_2.13[44,45] that uses a Verlet leapfrog algorithm for integration.[46] Simulations were carried out in the canonical ensemble (i.e. NVT ensemble), and the thermostat derived by Berendsen and co-workers[47]was employed to maintain a constant temperature. Periodic boundary conditions were not used and all atom−atom interactions were directly included in the simulation by ensuring that the cutoffs for the force and energy calculations were greater than the diameter of the nanoparticles in all simulations by 10 Å. A time step of 5.0 fs was used and the simulations were carried out for 3 ns, sufficiently long to ensure that all of the systems (anatase, rutile, and brookite nanoparticles ranging in size from 2 to 6 nm) reached a steady state. However, 3 ns is a relatively short time and we cannot rule out a phase change from brookite and rutile to anatase for the smaller particles, or from anatase and brookite to rutile for the larger particles, that would occur over physically much longer time scales. On the basis of experimental kinetic studies,[12] for example, it was estimated that a phase change for particles of the sizes investigated in this work would typically lie in the microsecond or millisecond range.

TABLE 2: Experimental Unit Cell Parameters and Fractional Coordinates for Rutile, Anatase and Brookite[55]

phase	crystal system	space group	*a*, Å	*b*, Å	*c*, Å	*u*
rutile[55]	tetragonal	*P*42/*mnm*	4.594	4.594	2.959	0.305
anatase[56]	tetragonal	*I*41/*amd*	3.786	3.786	9.514	0.208
brookite[55]	orthorhombic	*Pcab*	9.166	5.436	5.135	

2.2.a. Initial Configurations. The commonly occurring polymorphs of titanium dioxide are rutile, anatase, and brookite. Perfect lattices of these phases were prepared by using the experimental lattice parameters given in Table 2, which were taken from the literature. Spheres with diameters ranging from 2 to 6 nm in each of the three phases were cut from these lattices. See Figure 1 for snapshots of the initial and final configuration of the 3 nm particles in all three phases. The origin was placed at the center of mass of each sphere. In all cases some of the surface oxygen ions or titanium ions were removed to ensure electroneutrality.

2.3. Determination of Simulated Powder X-ray Diffraction Patterns. The simulated powder X-ray diffraction patterns were determined by using Debye functional analysis as described in detail by Kazakov and co-workers.[48] The intensity, I, of the diffracted coherent radiation is determined by the Debye formula

$$I_k(b) = \sum_n \sum_{m \neq n} f_n(b) f_m(b) \sin(2\pi b r_{nm})/(2\pi b r_{nm}) \qquad (2)$$

where $b = 2\sin(\theta)/\lambda$ and λ is the wavelength of the incident radiation, 2θ is the scattering angle, and r_{nm} is the distance

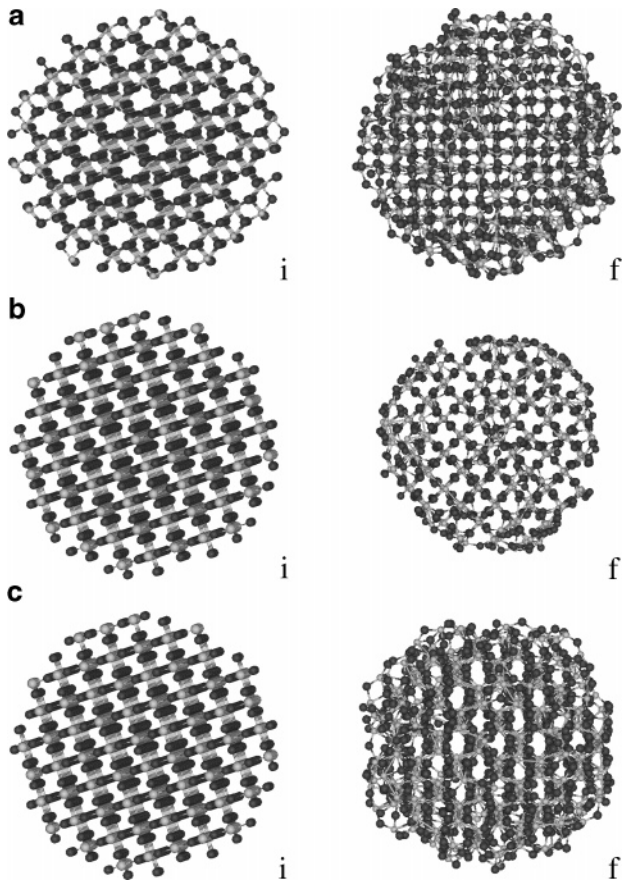

Figure 1. Snapshot of the initial (i) and final (f) structures at 300 K of 3 nm anatase nanoparticles (a), 3 nm rutile nanoparticles (b), and 3 nm brookite nanoparticles. Oxygen and titanium ions are dark and light colors, respectively.

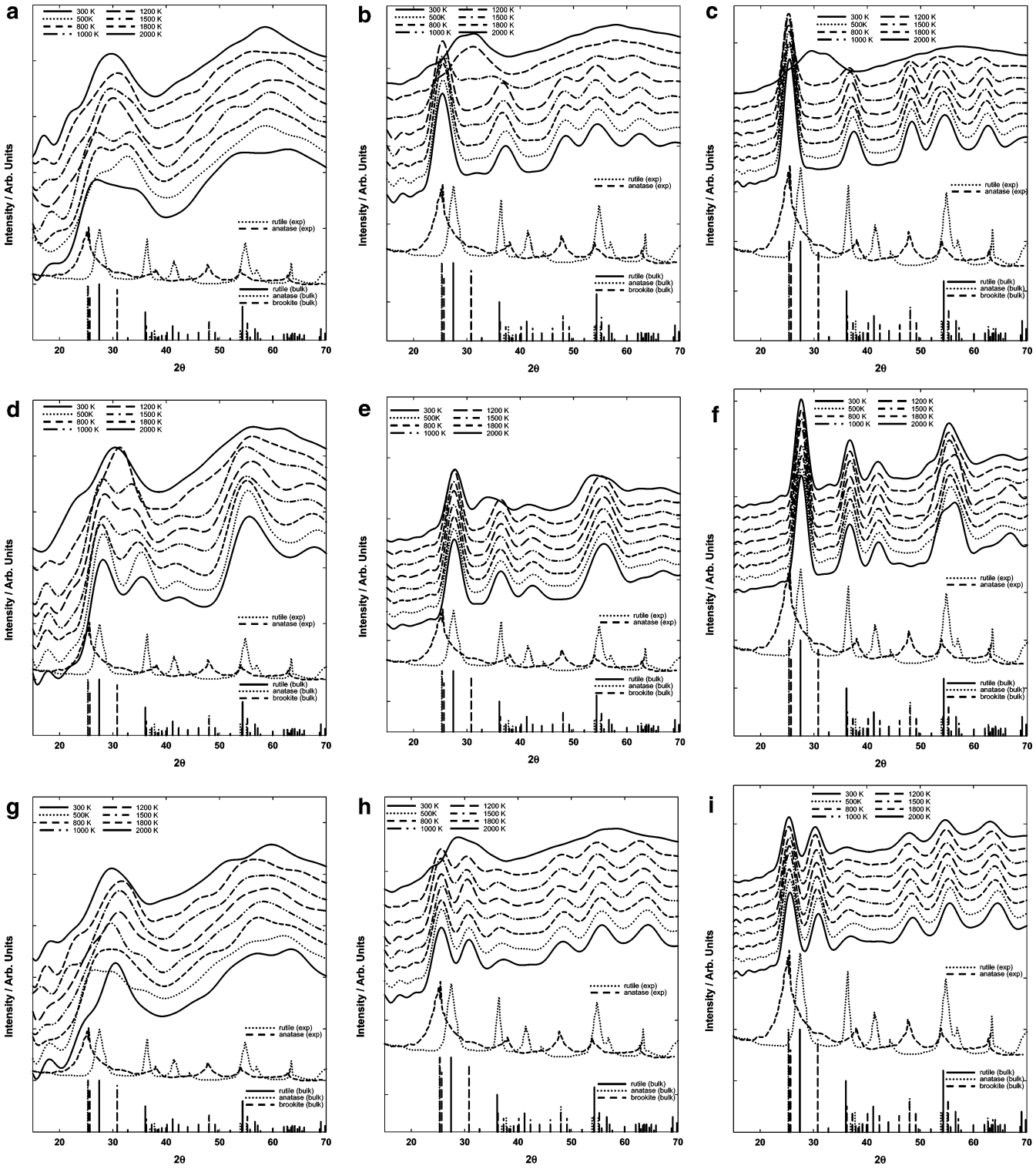

Figure 2. X-ray diffraction patterns of the final structure from Debye functional analysis eq 2: (a) 2 nm anatase; (b) 3 nm anatase; (c) 4 nm anatase; (d) 2 nm rutile; (e) 3 nm rutile; (f) 4 nm rutile; (g) 2 nm brookite; (h) 3 nm brookite; and (i) 4 nm brookite. In order from top to bottom: 2000, 1800, 1500, 1200, 1000, 800, 500, and 300 K. The experimental diffraction pattern for nanocrystalline rutile and anatase. The positions of the principal peaks in the experimental X-ray diffraction patterns for bulk anatase, bulk rutile, and bulk brookite are shown on the baseline.

between atoms n and m. The distance r_{nm} is easily determined from the coordinates generated by molecular dynamics. The functions $f_n(b)$ and $f_m(b)$ are the scattering factors for atoms n and m, respectively, and are calculated from the previously published data of Cromer and Mann.[49] The value of λ was taken to be that of the Cu Kα radiation (1.5418 Å). Some of the X-ray diffraction patterns at the different temperatures, sizes, and phases are shown in Figure 2.

3. Discussion

3.1. Structural Properties. The positions of the significant peaks in the X-ray diffraction patterns (both bulk and nanocrystalline material) of anatase and rutile obtained from the literature[50] are in excellent agreement with results from this work. From the X-ray diffraction patterns (see Figure 2) it can be seen that the reorganization due to surface formation has all but eliminated the structural features of the 2 nm particles. The

TABLE 3: Simulation Results for Heat Capacities, c_p, for the Nanoparticles from Eq 3

particle	$c_p(T)$, J mol^{-1} K^{-1}
2 nm anatase	$0.025T + 52.2$
3 nm anatase	$0.017T + 45.5$
4 nm anatase	$0.020T + 43.0$
2 nm brookite	$0.08T + 43.4$
3 nm brookite	$0.07T + 42.2$
4 nm brookite	$0.08T + 41.8$
2 nm rutile	$0.033T + 53.1$
3 nm rutile	$0.042T + 45.5$
4 nm rutile	$0.025T + 41.8$

principal peaks for 2 nm anatase, brookite, and rutile remain but the X-ray diffraction patterns of these particles do not show the same degree of ordering that is shown in the X-ray diffraction patterns of the larger particles. The bulk phase structural features present in the spectra are clearer for the larger particles. This is attributable to the fact that the surface atoms make up a smaller fraction of the total in larger particles.

The X-ray diffraction patterns indicate that individual nanoparticles investigated in this work do not spontaneously change phase during the course of the simulations. This is expected based on the kinetics of the phase transition that were determined experimentally and is of the order of microseconds or longer for the systems investigated in this work.[12]

The loss of the primary peaks (especially those at 25° in the X-ray diffraction pattern for anatase and brookite as well as that at 27.5° for rutile) as the temperature increases is an indication that the particles melt at temperatures lower than those observed for the bulk phase. As can be seen in Figure 2 these peaks persist to higher temperatures as the particles become larger. The principal peaks for rutile particles exist at a higher temperature than the peaks for anatase and brookite of a similar size. This loss of structure is expected as it is expected that ultrafine titanium dioxide should melt at a lower temperature than bulk titanium dioxide.[51] It should be noted that the reported melting point of bulk titanium dioxide is 2150 K.[31]

3.2. Heat Capacities. The heat capacity, c_p, is calculated from the potential energy and its relationship to temperature:[52]

$$c_p = \frac{dU}{dT} + \frac{3R}{2} \tag{3}$$

where U is the potential energy, T is the temperature, and R is the universal gas constant. A second-order polynomial was fitted to the potential energies and temperatures, taken from the simulations. In all cases the polynomial fitted the data to better than 0.1%. These polynomials were then differentiated with respect to temperature as described in eq 3 to yield the heat capacities. These heat capacities as a function of temperature are reported in Table 3. The experimental value of the heat capacity for nanocrystalline rutile (57.5 J mol^{-1} K^{-1}) at 300 K found in the literature[4,27] is in very good agreement with the values ranging from 63.0 to 49.3 J mol^{-1} K^{-1} found in this work for 2 nm rutile to 4 nm rutile. The differences in values can likely be attributed to the fact that the values reported in this work are for monodisperse titanium dioxide nanoparticles while the experimental data are for samples with polydispersity as indicated by the characterization method reported in the literature.[4,27] The results from the simulations confirm the trend reported in the literature,[4] viz., there is an increase in the heat capacity with an increase in temperature. The decrease in the value of the heat capacity with an increase in size as reported in the literature[4] was also observed in this work.

3.3. Coordination Environment and Bond Lengths. To determine the coordination number of the Ti ions, any oxygen ion within 2.3 Å of the Ti ion was considered bound to the Ti ion. The relationship between bond length and coordination environment as a function of size and phase is shown in Figure 3. The average or most probable bond length (see Table 4) is independent of phase and increases slightly with temperature, by about 0.01 Å for a 500 K increase in temperature. It is the coordination number of the titanium ion that is most sensitive to temperature, size, and phase. The relative percent of titanium ions that have a coordination number of 4, 5, or 6 for different particles at different temperatures is shown in Figure 4.

The experimental XAFS data of Chen et al.[32,33] for 5 nm anatase particles were interpreted by assuming that there are two different Ti−O bond lengths, 1.95 ± 0.02 and 1.77 ± 0.04 Å. The experimental data of Chen et al.[32,33] for 3 nm anatase particles were also interpreted by the assumption of two Ti−O bond lengths of 1.99 ± 0.02 and 1.84 ± 0.04 Å. In this work the most probable Ti−O bond length for the 6-coordinated titanium is 1.94 Å and the most probable Ti−O bond length for the 4-coordinated is titanium is 1.86 Å. Both of these values fall within the range determined by Chen et al.;[32,33] however, the greater structural detail that is available to molecular dynamics and not readily available to XAFS data reveals that a 5-coordinated titanium with a bond length of 1.92 Å should also be included in this picture of the microstructure of titanium dioxide nanoparticles.

The number of titanium ions that are not octahedral is greater for the smaller particles as expected and this is in principle in agreement with the interpretation of experimental data reported by Chen et al.,[32,33] who report that the shorter bond length occurs for 17% of the Ti−O units in a 5 nm particle and 20% in a 3 nm particle, which is different from the values reported in this work (see Figure 4). The main reason for this difference is the omission of the intermediate bond length characteristic of the 5-coordinated titanium in the interpretation of the experimental data.

To understand how the data of Chen et al.[32,33] can be related to this work, the Ti−O bond lengths for the 3 and 5 nm anatase particles were sorted from shortest to longest. For the 3 nm anatase nanoparticle the first 20% and the remaining 80% of the bond lengths were averaged to obtain two bond lengths with values of 1.85 Å (1.84 ± 0.04 Å) and 1.97 Å (1.99 ± 0.02 Å), respectively, which are in excellent agreement with the two bond lengths suggested by Chen et al.,[32,33] shown in parentheses. Taking a similar approach for the 5 nm particle in which the shortest 17% and the remaining 83% of the sorted Ti−O bond lengths were averaged, two bonds of length 1.81 (1.77 ± 0.04 Å) and 1.97 Å (1.95 ± 0.02 Å) were obtained and are again in good agreement with the values suggested by XAFS data.

3.4. Surface Energies. The calculation of the surface energy for different particle sizes makes it possible to understand the effect of curvature on the surface energy. Visual inspection (see Figure 1) of the particles indicated that they were almost spherical hence the surface area was calculated assuming spherical particles. Hence, the surface energies, $U_{surface}$, were calculated by using[53]

$$U_{surface} = \frac{U_{cluster} - nU_{bulk}}{4\pi r^2} \tag{4}$$

where $U_{cluster}$ is the potential energy of the nanoparticle, U_{bulk} is the potential energy per TiO_2 unit in the bulk material, n is the number of TiO_2 units in the nanoparticle, and r is the radius of the nanoparticle. It should be noted that eq 4 for the surface energy is the modified form of the corresponding equation in

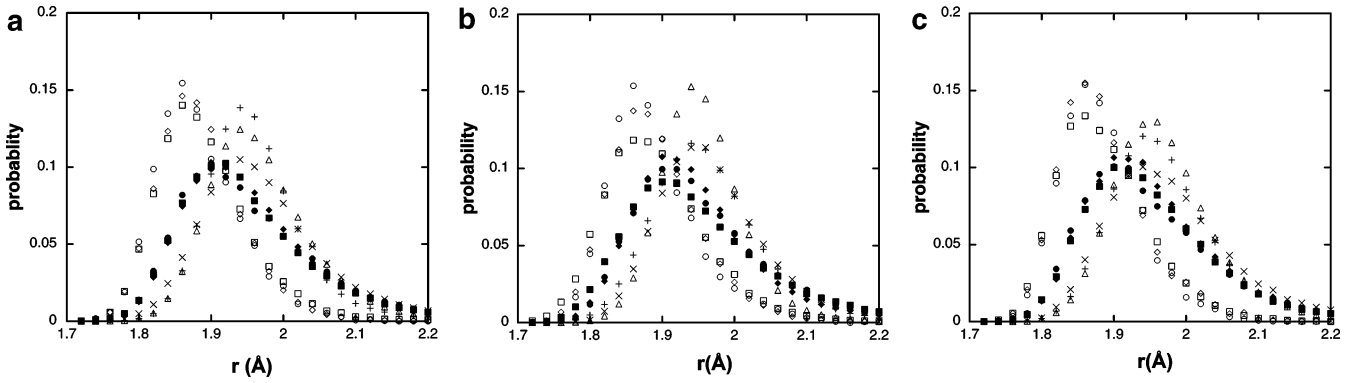

Figure 3. Ti−O bond length for anatase nanoparticles (a), rutile nanoparticles (b), and brookite nanoparticles (c) as a function of size and coordination number at 300 K from simulation: ○, 4-coordinated titanium in 2 nm particles; ●, 5-coordinated titanium in 2 nm particles; ×, 6-coordinated titanium in 2 nm particles; □, 4-coordinated titanium in 3 nm particles; ■, 5-coordinated titanium in 3 nm particles; +, 6-coordinated titanium in 3 nm particles; ◇, 4-coordinated titanium in 4 nm particles; ◆, 5-coordinated titanium in 4 nm particles; and △, 6-coordinated titanium in 4 nm particles.

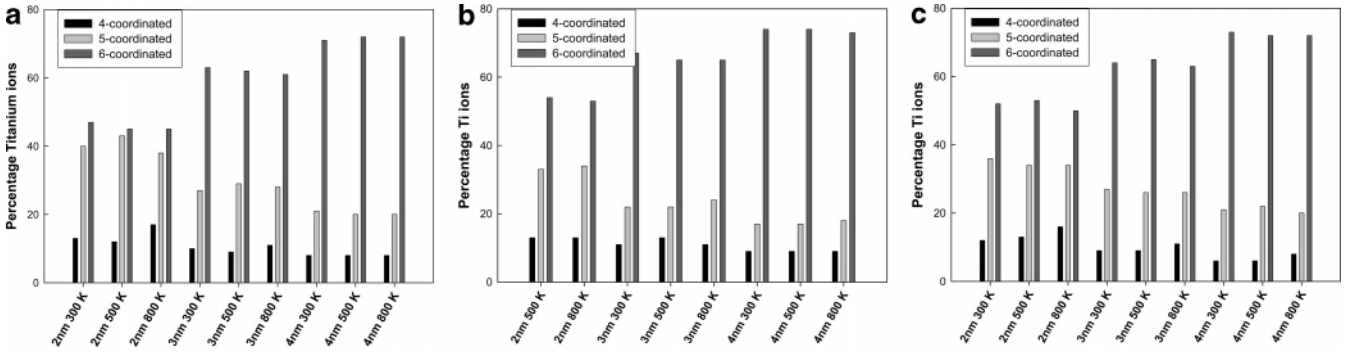

Figure 4. Percentage of titanium ions that are 4, 5, or 6 coordinated as a function of size and temperature for anatase nanoparticles (a), rutile nanoparticles (b), and brookite nanoparticles (c) from simulation.

TABLE 4: Most Probable Bond Lengths as a Function of Coordinate Number, Size, and Phase at 300 K from Simulation

diameter, nm	bond length, Å		
	4-coordinated Ti	5-coordinated Ti	6-coordinated Ti
	anatase		
2	1.860	1.895	1.940
3	1.863	1.915	1.945
4	1.865	1.905	1.943
5	1.870	1.905	1.945
6	1.865	1.910	1.945
	rutile		
2	1.860	1.910	1.955
3	1.865	1.905	1.945
4	1.868	1.905	1.945
5	1.865	1.915	1.952
6	1.868	1.900	1.920
	brookite		
2	1.862	1.905	1.940
3	1.858	1.905	1.945
4	1.862	1.905	1.952
5	1.870	1.910	1.950
6	1.865	1.912	1.952

ref 43. The modification takes into account that the surface energy for a spherical particle is calculated in this work as opposed to calculation of the surface energy for planar surfaces in ref 43. The surface energies are reported in Table 5 and plotted against the diameter of the particle at 300 K in Figure 5. The surface energy increases as the diameter of the particles increases (see Figure 5) and approaches a maximum. On the basis of the standard deviations in the potential energies, the surface energies were accurate to within 0.03 J m^{-2}; however,

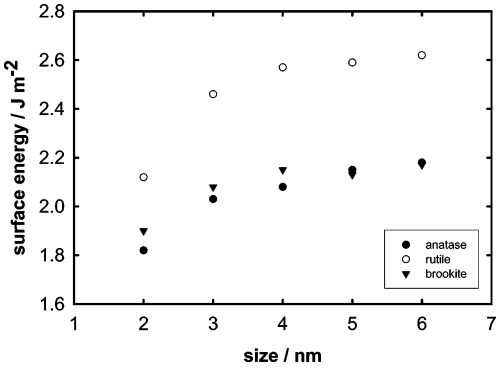

Figure 5. Surface energies as a function of particle diameter at 300 K (data shown in Table 5).

TABLE 5: Surface Energies for Nanoparticles as a Function of Size at 300 K from Simulation

diameter, nm	surface energies, J m^{-2}		
	anatase	rutile	brookite
2	1.82	2.12	1.90
3	2.03	2.46	2.08
4	2.08	2.57	2.15
5	2.15	2.59	2.13
6	2.18	2.62	2.17

this must take into consideration that the surface area of the particles was calculated with use of the initial diameters.

The only previously reported data on the surface energies for titanium dioxide were determined by atomistic simulation of rutile and anatase planar surfaces, which were calculated by using the corresponding equation to eq 4.[53] The surface energies reported for the planar rutile[54]{011}, {110}, {100}, and {221}

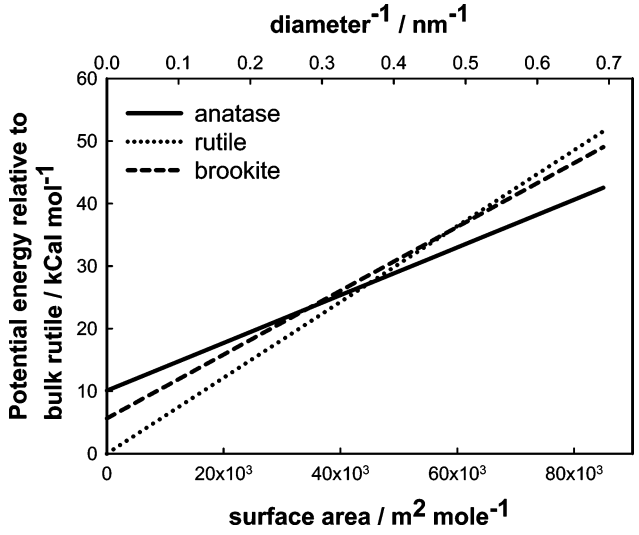

Figure 6. Energy of particles relative to bulk rutile as a function of surface area at 300 K from simulation.

faces are 1.85, 1.78, 2.08, and 2.02 J m^{-2}, respectively, and the surface energies from the literature for planar anatase {011} and {101} faces are 1.40 and 1.28 J m^{-2}, respectively. These values compare very well with values obtained in this work for the nanoparticles; however, it must be remembered that for large particles the total surface energy is dominated by the low index surfaces which have low surface energies, and for the smaller particles that approach the nanometer scale the contribution of high-index, high-energy surfaces becomes significant hence the surface energies are raised. There were no reported data for brookite. From the literature it can be seen that the surface energy for the low-index surfaces of microscopic (or larger) rutile is much higher than the surface energy for the low-index surfaces of microscopic (or larger) anatase. This trend is in agreement with what has been observed here, as the surface energies of rutile nanoparticles are higher than the surface energy for the corresponding size anatase nanoparticles. It must be noted that the contribution of surface energy to the total energy of a nanoparticle is very significant while for large particles the contribution of the surface energy to the total energy is negligible.

3.5. Relative Energies. A plot of the energies relative to bulk rutile at 300 K as a function of surface area is shown in Figure 6. When the surface areas of the particles are large (small particles), anatase is the more stable phase as opposed to the bulk phase where rutile is the most stable phase. This observation is well supported by the literature[5] which reports that in nanocrystalline titanium dioxide in which the individual particles are less than ~14 nm, anatase is the most stable phase. Note, however, that in this work the crossover in phase stability occurs for particles ~2.5 nm. The reason for the crossover in phase stability between anatase and rutile in the bulk versus nanocrystalline titanium dioxide is that the surface energy contribution to the total energy for rutile particles is higher than the surface energy contribution for anatase particles. When the particles become larger the surface energy becomes less important; hence for large enough particles the surface contribution becomes negligible and rutile becomes the more stable phase. This is easily rationalized if we consider that the surface energy per surface unit does not drop significantly when size increases but that the contribution of surface energy to the overall energy becomes negligible when the particle size increases because the bulk of the particle dominates the overall energy.

4. Conclusion

The formation of a surface on titanium dioxide nanoparticles has a profound effect on the stability of the nanoparticles and is the major factor causing anatase to be more stable in nanocrystalline form. Also evident from these simulations is the presence of four- and five-coordinated titanium ions, which have a shorter Ti−O bond length of 1.86 and 1.92 Å, respectively. These lower coordination Ti ions are found only at the surface of the nanoparticles.

Over the course of the simulations (3 ns), the isolated 2 nm titanium dioxide nanoparticles do not spontaneously transform phase from rutile and brookite to anatase even though there is a thermodynamic driving force to do so. In fact Boltzmann statistics tell us that the most probable conformation at equilibrium (infinite time) will be the lower energy state (anatase). The absence of this transformation is clearly due to the short time scale of the simulation, and in future work we plan to explore the application of simulation techniques that can explore these longer time scales, as well as transformations that might arise from interaction between the nanoparticles and their environment or with each other.

Acknowledgment. Funding was provided by an NSF grant (EAR-0123967). This research used resources of the National Energy Research Scientific Computing Center, which is supported by the Office of Science of the U.S. Department of Energy under Contract No. DE-AC03-76SF0098. This research also used resources at the Center for Computational Sciences Division, Oak Ridge National Laboratory, and Office of Advanced Scientific Computing Research, U.S. Department of Energy, under Contract No. DE-AC05-00OR22725 with UT-Battelle, LLC.

References and Notes

(1) Kroto, H. W.; Heath, J. R.; O'Brien, S. C.; Curl, R. F.; Smalley, R. E. *Nature* (*London*) **1985**, *318*, 162.
(2) Teo, B. K.; Shi, X.; Zhang, H. *J. Am. Chem. Soc.* **1991**, *113*, 4329.
(3) Diefenbach, J.; Martin, T. P. *J. Chem. Phys.* **1985**, *83*, 4585.
(4) Zhang, H.; Banfield, J. F. *Nanostruct. Mater.* **1998**, *10*, 185.
(5) Zhang, H.; Banfield, J. F. *J. Mater. Chem.* **1998**, *8*, 2073.
(6) Zhang, H.; Banfield, J. F. *Mater. Res. Soc. Symp. Proc.* **1998**, *481*, 619.
(7) Zhang, H.; Banfield, J. F. *Am. Mineral.* **1999**, *84*, 528.
(8) Zhang, H.; Banfield, J. F. *J. Mater. Res.* **2000**, *15*, 437.
(9) Zhang, H.; Banfield, J. F. *J. Phys. Chem. B* **2000**, *104*, 3481.
(10) Zhang, R.; Gao, L. *Mater. Res. Bull.* **2001**, *36*, 1957.
(11) Zhang, H.; Finnegan, M.; Banfield, J. F. *Nano Lett.* **2001**, *1*, 81.
(12) Zhang, H.; Banfield, J. F. *Chem. Mater.* **2002**, *14*, 4145.
(13) Zhu, X.; Birringer, R.; Herr, U.; Gleiter, H. *Phys. Rev. B*: *Condens. Matter Mater. Phys.* **1987**, *35*, 9085.
(14) Zachariah, M. R.; Carrier, M. J.; Blaisten-Barojas, E. *J. Phys. Chem.* **1996**, *100*, 14856.
(15) Tolbert, S. H.; Alivisatos, A. P. *J. Chem. Phys.* **1995**, *102*, 4642.
(16) Hendy, S. C.; Hall, B. D. *Phys. Rev. B*: *Condens. Matter Mater. Phys.* **2001**, *64*, 085425/1.
(17) Huang, J.; Bartell, L. S. *J. Mol. Struct.* **2001**, *567*−*568*, 145.
(18) Siegel, R. W.; Ramasamy, S.; Hahn, H.; Li, Z.; Lu, T.; Gronsky, R. *J. Mater. Res.* **1988**, *3*, 1367.
(19) Siegel, R. W. *Phys. Today* **1993**, *46*, 64.
(20) De Heer, W. A.; Knight, W. D.; Chou, M. Y.; Cohen, M. L. *Solid State Phys.* **1987**, *40*, 93.
(21) Steigerwald, M. L.; Alivisatos, A. P.; Gibson, J. M.; Harris, T. D.; Kortan, R.; Muller, A. J.; Thayer, A. M.; Duncan, T. M.; Douglass, D. C.; Brus, L. E. *J. Am. Chem. Soc.* **1988**, *110*, 3046.
(22) Ranade, M. R.; Navrotsky, A.; Zhang, H. Z.; Banfield, J. F.; Elder, S. H.; Zaban, A.; Borse, P. H.; Kulkarni, S. K.; Doran, G. S.; Whitfield, H. J. *Proc. Natl. Acad. Sci. U.S.A.* **2002**, *99*, 6476.
(23) Post, J. E.; Burnham, C. W. *Am. Mineral.* **1986**, *71*, 142.
(24) Mostoller, M.; Wang, J. C. *Phys. Rev. B*: *Condens. Matter Mater. Phys.* **1985**, *32*, 6773.
(25) Sawatari, H.; Iguchi, E.; Tilley, R. J. D. *J. Phys. Chem. Solids* **1982**, *43*, 1147.

(26) Catlow, C. R. A.; James, R. *Proc. R. Soc. London, Ser. A* **1982**, *384*, 157.
(27) de Ligny, D.; Richet, P.; Westrum, E. F., Jr.; Roux, J. *Phys. Chem. Miner.* **2002**, *29*, 267.
(28) Swamy, V.; Gale, J. D.; Dubrovinsky, L. S. *J. Phys. Chem. Solids* **2001**, *62*, 887.
(29) Swamy, V.; Gale, J. D. *Phys. Rev. B*: *Condens. Matter Mater. Phys.* **2000**, *62*, 5406.
(30) Ogata, S.; Iyetomi, H.; Tsuruta, K.; Shimojo, F.; Kalia, R. K.; Nakano, A.; Vashishta, P. *J. Appl. Phys.* **1999**, *86*, 3036.
(31) Collins, D. R.; Smith, W.; Harrison, N. M.; Forester, T. R. *J. Mater. Chem.* **1997**, *7*, 2543.
(32) Chen, L. X.; Rajh, T.; Jager, W.; Nedeljkovic, J.; Thurnauer, M. C. *J. Synchrotron Radiat.* **1999**, *6*, 445.
(33) Chen, L. X.; Rajh, T.; Wang, Z.; Thurnauer, M. C. *J. Phys. Chem. B* **1997**, *101*, 10688.
(34) Rajh, T.; Poluektov, O.; Dubinski, A. A.; Wiederrecht, G.; Thurnauer, M. C.; Trifunac, A. D. *Chem. Phys. Lett.* **2001**, *344*, 31.
(35) Collins, D. R.; Smith, W.; Harrison, N. M.; Forester, T. R. *J. Mater. Chem.* **1996**, *6*, 1385.
(36) Catlow, C. R. A.; Freeman, C. M.; Royle, R. L. *Physica B + C* **1985**, *131*, 1.
(37) Urusov, V. S.; Dubrovinskii, L. S.; Vasserman, E. A.; Eremin, N. N. *Kristallografiya* **1994**, *39*, 446.
(38) le Roux, H.; Glasser, L. *J. Mater. Chem.* **1997**, *7*, 843.
(39) Collins, D. R.; Smith, W. Technical Report DL-TR-96-001: Evaluation of TiO2 Force Fields; Council for the Central Laboratory of Research Councils, 1996.
(40) Matsui, M.; Akaogi, M. *Mol. Simul.* **1991**, *6*, 239.
(41) Streitz, F. H.; Mintmire, J. W. *J. Adhes. Sci. Technol.* **1994**, *8*, 853.
(42) Lewis, G. V.; Catlow, C. R. A. *J. Phys. C*: *Solid State Phys.* **1985**, *18*, 1149.
(43) Kim, D.-W.; Enomoto, N.; Nakagawa, Z.-e. *J. Am. Ceram. Soc.* **1996**, *79*, 1095.
(44) Smith, W. *J. Mol. Graph.* **1987**, *5*, 71.
(45) Smith, W.; Forester, T. R. *J. Mol. Graph.* **1996**, *14*, 136.
(46) Allen, M. P.; Tildesley, D. J. *Computer Simulation of Liquids*; Claredon Press: Oxford, UK, 1987.
(47) Berendsen, H. J. C.; Postma, J. P. M.; Vangunsteren, W. F.; Dinola, A.; Haak, J. R. *J. Chem. Phys.* **1984**, *81*, 3684.
(48) Kazakov, A. V.; Shpiro, E. S.; Voskoboinikov, T. V. *J. Phys. Chem.* **1995**, *99*, 8323.
(49) Cromer, D. T.; Mann, J. B. *Acta Crystallogr., Sect. A*: *Cryst. Phys. Diffr., Theor. Gen. Crystallogr.* **1968**, *24*, 321.
(50) Wang, C.; Deng, Z. X.; Li, Y. *Inorg. Chem.* **2001**, *40*, 5210.
(51) Zhao, S. J.; Wang, S. Q.; Cheng, D. Y.; Ye, H. Q. *J. Phys. Chem. B* **2001**, *105*, 12857.
(52) Wang, L.; Zhang, Y.; Xiufang, B.; Chen, Y. *Phys. Lett. A* **2003**, *A 310*, 197.
(53) Oliver, P. M.; Watson, G. W.; Kelsey, E. T.; Parker, S. C. *J. Mater. Chem.* **1997**, *7*, 563.
(54) Bredow, T. *Int. J. Quantum Chem.* **1999**, *75*, 127.
(55) Wyckoff, R. W. G. *Crystal Structures. Vol. 1. 2nd ed*, 1963.
(56) Howard, C. J.; Sabine, T. M.; Dickson, F. *Acta Crystallogr., Sect. B: Struct. Sci.* **1991**, *B47*, 462.